

Multi-symplectic discretisation of wave map equations

David Cohen^{*1,2} and Olivier Verdier^{†1,3}

¹*Department of Mathematics and Mathematical Statistics, Umeå, Sweden*

²*Department of Mathematics, University of Innsbruck, Austria*

³*Department of Computing, Mathematics and Physics, Bergen University College, Norway*

2018-08-24

We present a new multi-symplectic formulation of constrained Hamiltonian partial differential equations, and we study the associated local conservation laws. A multi-symplectic discretisation based on this new formulation is exemplified by means of the Euler box scheme. When applied to the wave map equation, this numerical scheme is explicit, preserves the constraint and can be seen as a generalisation of the SHAKE algorithm for constrained mechanical systems. Furthermore, numerical experiments show excellent conservation properties of the numerical solutions.

Keywords Constrained Hamiltonian partial differential equations · Wave map equations · Multi-symplectic partial differential equation · Numerical discretisation · Multi-symplectic schemes · Euler box scheme

Mathematics Subject Classification (2010) 35Q51 · 35Q53 · 37K05 · 37K10 · 37M15 · 65M06 · 65M99 · 65P10

1. Introduction

Ever since the seminal papers [20] and [8] on multi-symplectic Hamiltonian PDEs and their discretisation, there has been a growing interest in multi-symplectic integrators. The purpose of this paper is to propose a novel multi-symplectic integrator for multi-symplectic partial differential equations (PDEs) with constraints. For an overview of multi-symplectic PDEs, we refer to [7, 8, 19], and references therein.

*david.cohen@umu.se

†olivier.verdier@hib.no

We illustrate our findings with a particular multi-symplectic PDE with constraints, the wave map equation on the sphere (or on the circle):

$$\begin{aligned} u_{tt}(x, t) - \Delta u(x, t) &= \lambda u(x, t) \quad \text{in } \Omega \times (0, \infty) \\ \|u(x, t)\|^2 &= 1 \\ u(x, 0) &= u_0(x), \quad u_t(x, 0) = v_0(x), \end{aligned} \tag{1}$$

where the *domain* $\Omega \subset \mathbb{R}^m$ is an m -dimensional box or torus, $u \in \mathbb{S}^\ell$ so the *target manifold* \mathbb{S}^ℓ is the ℓ -dimensional sphere, and λ is a Lagrange multiplier. Here, the initial position u_0 and velocity v_0 (living in the tangent space of the target manifold) of the wave are given. Note that we will allow the “sphere” to be a hyperbolic sphere, as we allow the norm on $\mathbb{R}^{\ell+1}$ to be degenerate.

In the particular situation of the standard wave map equation (1), our general multi-symplectic method takes the simple form

$$\begin{aligned} \frac{u^{n,i+1} - 2u^{n,i} + u^{n,i-1}}{\Delta t^2} - \frac{u^{n+1,i} - 2u^{n,i} + u^{n-1,i}}{\Delta x^2} &= -\lambda^{n,i+1} u^{n,i} \\ \|u^{n,i+1}\|^2 &= 1, \end{aligned} \tag{2}$$

where $u^{n,i} \approx u(x_n, t_i)$ on a uniform rectangular grid with meshes Δx and Δt . This method can thus be regarded as a particular case of the SHAKE algorithm for constrained mechanical systems [13, Sect. VII.1.4] [21], to Hamiltonian PDEs with constraints.

The advantages of the proposed multi-symplectic method, which for the standard wave map equation reduces to (2), are summarized as follows:

- The implementation of the numerical method is effortless;
- It has no energy drift;
- It is explicit for the wave map equation on the sphere;
- We can simulate wave map equations with an additional smooth potential;
- We can handle arbitrary target Riemannian submanifolds of \mathbb{R}^n , where \mathbb{R}^n is equipped with a nondegenerate bilinear form.

The wave map equation (1) has received considerable attention, from a more theoretical point of view, during the last decades. It has applications in general relativity and in particle physics, see [28, 25, 34, 2] and references therein for details. Furthermore, this equation is integrable for a domain of dimension one ($m = 1$) [3], or when the target manifold is a circle; has a conserved energy; is time reversible; is non dissipative; is invariant with respect to the scaling $u(x, t) \rightarrow u(\gamma x, \gamma t)$ for $\gamma \in \mathbb{R}$; is related to Einstein equations [5]; is related to the sine-Gordon equation [24, 28]; has critical regularity $m/2$; possesses, for example, global smooth solutions if the initial data are smooth and if the domain is \mathbb{R}^1 [32, 33, 29, 30, 16, 35]; has blow-up solutions in finite time if the domain is \mathbb{R}^m with $m \geq 3$ [17, 18]; it is however an open problem to show if smooth solutions do become singular in finite time; etc. See also [31, 34] and references therein.

We now review the literature on the numerical analysis of the wave map equation. The earlier papers [6, 14] report numerical evidence of finite-time blow-up of smooth initial data. These works restrict to equivariant maps, where the wave map equation reduces to a semilinear scalar wave equation. This scalar problem is then discretised with the standard leapfrog scheme or the Crank–Nicholson scheme with adaptive mesh. Very recently, there has been a renewed interest for the numerical discretisation of wave map problems starting with the series of papers [3, 2, 4, 1]. These works prove convergence of certain (semi)-implicit finite element based methods to weak solutions of wave map equations. The main aim of [23] is to compare the evolution of (the blow-up of) equivariant maps using the classical Runge–Kutta 4 scheme and the RATTLE algorithm for the time discretisation of wave map equations. Here, the authors used the method of lines to discretise the PDE and a five-point formulae for the spatial derivatives. Our multi-symplectic numerical method shares similarities with the RATTLE algorithm (as we shall see in §3 that it is the SHAKE algorithm in time, and RATTLE is almost identical to SHAKE [21, §5.1.2]) but we would like to point out that our formalism is more general than the one proposed in [23]. In addition, the authors of the previously cited paper analyse, for the first time, the blow-up dynamics and singularity formation in the nonequivariant case using the same numerical methods in reference [10]. Furthermore, the recent publication [15] presents a finite difference method applied to a reformulation of the wave map equation. The proposed method conserves the energy, the constraint and converges to the weak solution of the wave map equation. This numerical method is however implicit.

The paper is organised as follows. §2 presents new multi-symplectic formulation and discretisation of general Hamiltonian PDEs with constraint. This is then illustrate for the particular case of wave map equations in §3 and §4. The paper ends with concluding remarks in §5 and with explanations on how to simulate wave map equations where the target manifold is the complex projective space in Appendix A.

2. Multi-symplectic Hamiltonian PDEs with constraint

We begin by extending the concept of multi-symplectic PDEs to multi-symplectic PDEs with constraint. We will then use this new multi-symplectic formulation to derive a multi-symplectic numerical scheme for the above type of problems.

2.1. Multi-symplectic formulation of the equations

There are two standard ways to construct multi-symplectic formulations of a PDE. One approach is using the Lagrangian formulation of the problem, see the early papers [12, 20] and references therein. The other approach is to write the partial differential equation as a system of equations containing only first-order derivatives in space and time, see equation (3) below, and then to extract the multi-symplectic structure, see the early papers [7, 8, 19] and references therein.

We will now generalise this second approach to PDEs with constraints. In order to do this, let n be an integer, two skew-symmetric matrices $M, K \in \mathbb{R}^{n \times n}$ and a scalar

function $S: \mathbb{R}^n \rightarrow \mathbb{R}$. We consider *Hamiltonian systems on a multi-symplectic structure with constraint*

$$\begin{aligned} Mz_t + Kz_x &= \nabla_z S(z) - \lambda \nabla g(z) \\ g(z) &= 0. \end{aligned} \tag{3}$$

Here, $z = z(x, t) \in \mathbb{R}^n$ is the state variable with components $z = (z_1, \dots, z_n)$. λ is a Lagrange multiplier, $x \in [0, 1]$ (for simplicity, see the remark below) and $t > 0$. The motion is thus constrained to satisfy $g(z) = 0$, where $g: \mathbb{R}^\ell \rightarrow \mathbb{R}$ and $\nabla g(z)$ denotes the gradient of g . Note that it is straightforward to generalize to the case of more than one constraint.

Remark that, one could add the Lagrange multiplier λ as a variable in z and add a zero row and column to M and K . this would give the standard multi-symplectic formulation. However, in general, a scheme derived with this direct reformulation of the equation will not be stable. This problem is well known in differential-algebraic equations: in general one has to enforce the constraint at the end step.

Observe that most multi-symplectic PDEs have removable constraints defining the auxiliary variables. However, in our paper, the constraint is imposed externally.

Remark 2.1. One can further treat the case $x = (x_1, x_2) \in [0, 1]^2$ (or any higher dimension) considering the multi-symplectic formulation

$$\begin{aligned} Mz_t + K_1 z_{x_1} + K_2 z_{x_2} &= \nabla_z S(z) - \lambda \nabla g(z) \\ g(z) &= 0 \end{aligned}$$

with three skew-symmetric matrices M, K_1 and K_2 . See for example §4.1.

2.2. Conservation laws

From the formulation (3), we shall now introduce the conservation laws of multi-symplecticity, energy and momentum. These derivations are similar to [19, Chap. 12] with the added difficulty of the fulfillment of the constraint.

Proposition 2.2. *The differential forms*

$$\omega := \frac{1}{2} dz \wedge M dz \quad \text{and} \quad \kappa := \frac{1}{2} dz \wedge K dz$$

satisfy the following conservation law of multi-symplecticity

$$\omega_t + \kappa_x = 0 \tag{4}$$

along the solutions of the multi-symplectic PDE (3).

Proof. Let us consider the variational equation of (3)

$$\begin{aligned} Mdz_t + Kdz_x &= S_{zz}(z)dz - d(\lambda \nabla g(z)) \\ \nabla g(z)dz &= 0. \end{aligned}$$

Taking the wedge product of the above expression with dz , one then obtains

$$dz \wedge Mdz_t + dz \wedge Kdz_x = dz \wedge S_{zz}(z)dz - dz \wedge (d\lambda \nabla g(z)) - dz \wedge (g_{zz}(z)dz)\lambda.$$

Using the symmetry of $S_{zz}(z)$, the symmetry of the Hessian matrix $g_{zz}(z)$, and using the constraint, we see that the right-hand side is equal to zero. Finally, applying properties of the wedge product, we observe that

$$\omega_t = \frac{1}{2}dz_t \wedge Mdz + \frac{1}{2}dz \wedge Mdz_t = -\frac{1}{2}Mdz_t \wedge dz + \frac{1}{2}dz \wedge Mdz_t = dz \wedge Mdz_t,$$

and similarly for the term κ_x . This gives the above conservation law of multi-symplecticity. \square

Observe that the conservation of symplecticity in [Proposition 2.2](#) amounts to a conservation of presymplecticity on the constraint submanifold. Note, however, that there is no consensus as to what presymplecticity and symplecticity are in the multi-symplectic case. In fact, most definitions of multi-symplecticity would correspond to presymplecticity in one independent variable. Studying in which way our methods are in fact multi-symplectic (in a stronger sense than presymplecticity) is outside the scope of this paper.

As noted in [\[22\]](#), the conservation law of multi-symplecticity [\(4\)](#) can be simplified by taking a non-unique splitting of the matrices M and K (see also [§ 2.3](#) below) such that

$$M = M_+ + M_-, \quad K = K_+ + K_-,$$

where

$$M_+^T = -M_- \quad \text{and} \quad K_+^T = -K_-.$$

Hence [\(4\)](#) holds with

$$\omega = dz \wedge M_+ dz \quad \text{and} \quad \kappa = dz \wedge K_+ dz.$$

One next obtains the conservation law of energy by taking the usual scalar product (denoted by $\langle \cdot, \cdot \rangle$) of [\(3\)](#) with z_t . Noting that $\langle z_t, Mz_t \rangle = 0$, one gets

$$\langle z_t, K_+ z_x + K_- z_x \rangle = \langle z_t, \nabla_z S(z) \rangle - \langle z_t, \lambda \nabla g(z) \rangle.$$

Since $\langle z_t, K_+ z_x + K_- z_x \rangle = \partial_x (\langle z_t, K_+ z \rangle) - \partial_t (\langle z_x, K_+ z \rangle)$ and $\langle z_t, \nabla_z S(z) \rangle = \partial_t (\nabla_z S(z))$, one obtains the *conservation law of energy*

$$E_t(z) + F_x(z) = 0$$

with the density functions

$$\begin{aligned} E(z) &= S(z) + \langle z_x, K_+ z \rangle \\ F(z) &= -\langle z_t, K_+ z \rangle. \end{aligned}$$

Similarly, the *conservation law of momentum* reads

$$I_t(z) + J_x(z) = 0$$

with the density functions

$$\begin{aligned} I(z) &= -\langle z_x, M_+ z \rangle \\ J(z) &= S(z) + \langle z_t, M_+ z \rangle. \end{aligned}$$

2.3. Multi-symplectic discretisation of Hamiltonian PDEs with constraint

The goal of this subsection is now to construct a numerical method for (3) which preserves a discrete analog of the conservation law of multi-symplecticity (4).

In order to do this, we first extend the Euler box scheme, see for example [22], to constrained Hamiltonian PDE (3). We set $\Delta x = x_{n+1} - x_n, n \in \mathbb{N}$, and $\Delta t = t_{i+1} - t_i$, for a nonnegative integer i . Moreover, we define the forward and backward differences in time

$$\delta_t^+ z^{n,i} = \frac{z^{n,i+1} - z^{n,i}}{\Delta t} \quad \text{and} \quad \delta_t^- z^{n,i} = \frac{z^{n,i} - z^{n,i-1}}{\Delta t},$$

and similarly for differences in space.

Further, we introduce a splitting of the two matrices M and K in (3), setting $M = M_+ + M_-$, $K = K_+ + K_-$ where $M_+^T = -M_-$ and $K_+^T = -K_-$. In this article, we only consider this particular splitting, keeping in mind that it is not the only possible splitting. We now apply the symplectic Euler method to the temporal and spatial discretisation of (3). This yields the *Euler box scheme for constrained Hamiltonian PDE* (3)

$$\begin{aligned} M_+ \delta_t^+ z^{n,i} + M_- \delta_t^- z^{n,i} + K_+ \delta_x^+ z^{n,i} + K_- \delta_x^- z^{n,i} &= \nabla_z S(z^{n,i}) - \lambda^{n,i+1} \nabla g(z^{n,i}) \\ g(z^{n,i+1}) &= 0, \end{aligned} \quad (5)$$

where $z^{n,i} \approx z(x_n, t_i)$ on a uniform rectangular grid.

To conclude this subsection, we show that the Euler box scheme (5) is a multi-symplectic integrator.

Proposition 2.3. *We consider the Euler box scheme (5) with $M_+^T = -M_-$ and $K_+^T = -K_-$. The Euler box scheme (5) for constrained Hamiltonian PDE (3) satisfies the following discrete multi-symplectic conservation law*

$$\delta_t^+ (dz^{n,i-1} \wedge M_+ dz^{n,i}) + \delta_x^+ (dz^{n-1,i} \wedge K_+ dz^{n,i}) = 0. \quad (6)$$

In analogy to the original definition of multi-symplectic integrators from [8], we thus call this numerical method a multi-symplectic integrator for (3).

Proof. The proof follows the lines of the proof of Proposition 2.2, see also the one of [22, Prop. 1] in the absence of constraints. We start the proof by considering the discrete variational equation

$$\begin{aligned} M_+ \delta_t^+ dz^{n,i} + M_- \delta_t^- dz^{n,i} + K_+ \delta_x^+ dz^{n,i} + K_- \delta_x^- dz^{n,i} &= S_{zz}(z^{n,i}) dz^{n,i} - d(\lambda^{n,i+1} \nabla g(z^{n,i})) \\ \nabla g(z^{n,i}) dz^{n,i} &= 0. \end{aligned}$$

Taking the wedge product of the above expression with $dz^{n,i}$, we obtain

$$\begin{aligned} dz^{n,i} \wedge (M_+ \delta_t^+ dz^{n,i} + M_- \delta_t^- dz^{n,i}) + dz^{n,i} \wedge (K_+ \delta_x^+ dz^{n,i} + K_- \delta_x^- dz^{n,i}) &= \\ dz^{n,i} \wedge S_{zz}(z^{n,i}) dz^{n,i} - dz^{n,i} \wedge d\lambda^{n,i+1} \nabla g(z^{n,i}) - dz^{n,i} \wedge g_{zz}(z^{n,i}) dz^{n,i} \lambda^{n,i+1}. \end{aligned}$$

Using properties of the wedge product, the symmetry of $S_{zz}(z)$ and of the Hessian matrix $g_{zz}(z)$, and the fact that the numerical solution given by (5) satisfies the constraint, we end up with the discrete conservation law (6). \square

3. Applications to wave map equations

In this section, we show that the wave map equation possesses a multi-symplectic formulation. Furthermore, we derive an Euler box scheme for the wave map equation and show that this multi-symplectic numerical method is explicit, and has a particular simple form which is closely related to the SHAKE algorithm.

3.1. A multi-symplectic formulation of wave map equations

The following wave map equations with a smooth potential V [30, 11, 38]

$$\begin{aligned} u_{tt} - u_{xx} &= -V'(u) + \lambda \nabla g(u) \\ g(u) &= 0, \end{aligned} \tag{7}$$

where $u = (u_1, u_2, u_3) \in \mathbb{R}^3$, can be put into the multi-symplectic framework (3). For simplicity, we will only consider a domain in \mathbb{R}^1 here. An example on a 2-dimensional torus will be given in §4.

Indeed, considering the vector of state variable $z = (u_1, u_2, u_3, v_1, v_2, v_3, m_1, m_2, m_3)$, taking the skew-symmetric matrices (I denotes the identity matrix in \mathbb{R}^3)

$$M = \begin{pmatrix} 0 & -I & 0 \\ I & 0 & 0 \\ 0 & 0 & 0 \end{pmatrix} \quad \text{and} \quad K = \begin{pmatrix} 0 & 0 & -I \\ 0 & 0 & 0 \\ I & 0 & 0 \end{pmatrix}$$

and considering the scalar function $S(z) = \frac{1}{2}(v_1, v_2, v_3)^T(v_1, v_2, v_3) - \frac{1}{2}(m_1, m_2, m_3)^T(m_1, m_2, m_3) + V(u_1, u_2, u_3)$ we obtain the equivalent representation (3). This multi-symplectic formulation of the wave map equation (7) takes the explicit form

$$\begin{aligned} -v_t - m_x &= V'(u) - \lambda \nabla g(u) \\ u_t &= v \\ u_x &= -m \\ g(u) &= 0. \end{aligned}$$

In particular, taking $V \equiv 0$ and $g(u) = |u|^2 - 1$ in (7), one gets a multi-symplectic formulation (3) of the classical wave map problem into the unit sphere [31]

$$\begin{aligned} u_{tt} - u_{xx} &= \lambda u \\ |u|^2 &= 1. \end{aligned} \tag{8}$$

For the wave map equation (7), we choose the splitting of the matrices

$$M_+ = \begin{pmatrix} 0 & -I & 0 \\ 0 & 0 & 0 \\ 0 & 0 & 0 \end{pmatrix} \quad \text{and} \quad K_+ = \begin{pmatrix} 0 & 0 & -I \\ 0 & 0 & 0 \\ 0 & 0 & 0 \end{pmatrix}.$$

The conservation laws of multi-symplecticity, energy and momentum then read

$$\begin{aligned} (du \wedge dv)_t + (du \wedge dm)_x &= 0 \\ \left(\frac{1}{2}v^T v - \frac{1}{2}m^T m + V(u) - (m_x)^T m\right)_t + ((u_t)^T m)_x &= 0 \\ ((u_x)^T v)_t + \left(\frac{1}{2}v^T v - \frac{1}{2}m^T m + V(u) - (u_t)^T v\right)_x &= 0. \end{aligned}$$

Integrating these two last conservation laws over the spatial domain and using appropriate boundary conditions, one obtains two conserved quantities. Wave map problems (7) are thus Hamiltonian PDEs with constraint and having the following conserved quantities, see also [34, 3],

$$\begin{aligned} H(u) &= \int_{\Omega} \left(\frac{1}{2}|u_t|^2 + \frac{1}{2}|u_x|^2 + V(u)\right) dx \\ M(u) &= \int_{\Omega} \frac{1}{2}(u_x)^T u_t dx. \end{aligned}$$

3.2. A multi-symplectic scheme for wave map equations

For the particular case of wave map problems (7), one can eliminate all the additional variables in the Euler box scheme (5) and express the numerical scheme only in terms of u . This gives us the following multi-symplectic integrator for wave map equations (7)

$$\begin{aligned} \delta_t^+ \delta_t^- u^{n,i} - \delta_x^+ \delta_x^- u^{n,i} &= -V'(u^{n,i}) - \lambda^{n,i+1} \nabla g(u^{n,i}) \\ g(u^{n,i+1}) &= 0. \end{aligned}$$

Developing all the above terms, the Euler box scheme for wave map equations (7) thus reads

$$\begin{aligned} \frac{u^{n,i+1} - 2u^{n,i} + u^{n,i-1}}{\Delta t^2} - \frac{u^{n+1,i} - 2u^{n,i} + u^{n-1,i}}{\Delta x^2} &= -V'(u^{n,i}) - \lambda^{n,i+1} \nabla g(u^{n,i}) \\ g(u^{n,i+1}) &= 0. \end{aligned}$$

It is more convenient to rewrite it in the equivalent form (with a slight abuse of notation for the Lagrange multiplier $\lambda^{n,i+1}$):

$$\begin{aligned} \frac{\widetilde{u^{n,i+1}} - 2u^{n,i} + u^{n,i-1}}{\Delta t^2} - \frac{u^{n+1,i} - 2u^{n,i} + u^{n-1,i}}{\Delta x^2} &= -V'(u^{n,i}) \\ u^{n,i+1} = \widetilde{u^{n,i+1}} - \lambda^{n,i+1} \nabla g(u^{n,i}) & \quad (9) \\ g(u^{n,i+1}) &= 0. \end{aligned}$$

The last formulation emphasizes that the computation consists of two steps:

1. Compute $\widetilde{u^{n,i+1}}$ using the explicit formula (9)

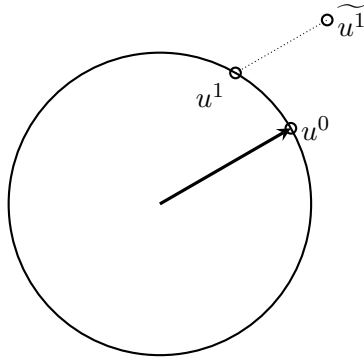


Figure 1: The point u^1 is obtained by first computing a point \widetilde{u}^1 by ignoring the constraint. We then project the point \widetilde{u}^1 along the direction of u^0 , to obtain a point u^1 which fulfills the constraint. This means that we have $u^1 = \widetilde{u}^1 + \lambda u^0$ for some scalar λ . In the case of a quadratic constraint, the expression for λ is explicitly given by (10).

2. Project $\widetilde{u}^{n,i+1}$ onto the constraint manifold in the direction $\nabla g(u^{n,i})$.

In the classical wave map case, the constraint manifold is a sphere of radius one. The value of the Lagrange multiplier $\lambda^{n,i+1}$ is thus a solution of a quadratic problem.

We assume that u^0 (the first step of the scheme) lies on the sphere of radius one. One then computes a point \widetilde{u}^1 by ignoring the constraint, see Figure 1. If we first define $p = \|\widetilde{u}^1\|^2 - 1$ and $s = \langle u^0, \widetilde{u}^1 \rangle$, we straightforwardly obtain

$$\lambda = -s + \sqrt{s^2 - p}. \quad (10)$$

Note that, as s is generally positive, we use the following equivalent formula in order to avoid potential ‘‘catastrophic cancellation’’ issues: $\lambda = \frac{p}{-s - \sqrt{s^2 - p}}$. With either of those formulas the projection step is the explicit operation

$$u^1 = \widetilde{u}^1 - \frac{p}{-s - \sqrt{s^2 - p}} u^0$$

The numerical integrator (9) can also be seen as a particular instance of the SHAKE algorithm for constrained mechanical systems, see e.g. [21] or [13, Sect. VII.1.4], to wave map equations. In other words, (9) corresponds to an application of SHAKE to a finite difference discretisation of the wave equation by central finite differences.

One can wonder what happens to the hidden constraints. As the algorithm (9) for wave map equations is written in u only, the hidden constraints do not really make sense anymore. Notice, however, that the constraints in u are exactly preserved. Suppose that one had used the full Euler box scheme (5) instead, with unknown variable z . Then the time and space momenta, would be first order finite difference approximations of the time and space derivatives of the position u . The corresponding hidden constraints would thus be approximately preserved up to first order.

Observe that for other constrained PDEs (Hamiltonian or not), it is extremely difficult to give a precise definition of hidden constraints [26, 37].

4. Numerical experiments for wave map equations

This section illustrates the main properties of the Euler box scheme (9) when applied to the wave map equations (7) and (8).

These numerical experiments illustrate the following properties of our method:

1. We observe convergence of order two, and absence of energy drift for smooth solutions (§4.1);
2. We observe breather solutions accurately for several periods (§4.2);
3. We observe the correct blow-up time as in [15, 3] (§4.3);
4. We show that we can simulate the wave map equation with potential (§4.4);
5. We show the versatility of our approach by considering the Poincaré disk or the complex projective space as a target manifold, see also Appendix A.

4.1. Convergence rates and approximate energy conservation for the wave map from the torus to the circle

We consider the wave map problem (8) in two spatial dimensions [15]

$$\begin{aligned} u_{tt} - u_{x_1x_1} - u_{x_2x_2} &= \lambda u \\ |u|^2 - 1 &= 0, \end{aligned} \tag{11}$$

where $u = u(x_1, x_2, t) \in \mathbb{R}^2$, with $(x_1, x_2) \in \mathbb{T}^2$ the 2-dimensional torus.

For sake of completeness let us first state the multi-symplectic formulation and the scheme in the present setting. The above wave map problem has the following multi-symplectic formulation

$$\begin{aligned} Mz_t + K_1z_{x_1} + K_2z_{x_2} &= \nabla_z S(z) - \lambda \nabla g(u) \\ g(u) &= 0 \end{aligned}$$

with the state variable $z = (u, v, p_1, p_2)$, the function $S(z) = \frac{1}{2}v^T v - \frac{1}{2}p_1^T p_1 - \frac{1}{2}p_2^T p_2$, the constraint $g(u) = |u|^2 - 1$ and the three skew-symmetric matrices

$$M = \begin{pmatrix} 0 & -I & 0 & 0 \\ I & 0 & 0 & 0 \\ 0 & 0 & 0 & 0 \\ 0 & 0 & 0 & 0 \end{pmatrix} \quad \text{and} \quad K_1 = \begin{pmatrix} 0 & 0 & -I & 0 \\ 0 & 0 & 0 & 0 \\ I & 0 & 0 & 0 \\ 0 & 0 & 0 & 0 \end{pmatrix} \quad \text{and} \quad K_2 = \begin{pmatrix} 0 & 0 & 0 & -I \\ 0 & 0 & 0 & 0 \\ 0 & 0 & 0 & 0 \\ I & 0 & 0 & 0 \end{pmatrix}.$$

The corresponding multi-symplectic Euler box scheme, for the classical splitting of the matrices, reads

$$\begin{aligned} \delta_t^+ \delta_t^- u^{n,m,i} - \delta_{x_1}^+ \delta_{x_1}^- u^{n,m,i} - \delta_{x_2}^+ \delta_{x_2}^- u^{n,m,i} &= -\lambda^{n,i+1} \nabla g(u^{n,m,i}) \\ g(u^{n,m,i+1}) &= 0. \end{aligned} \tag{12}$$

Wavenumber	Amplitude	Phase
(1, 1)	1	0
(2, 1)	0.5	0.5
(-1, 1)	0.2	0.8

Table 1: The values of the wavenumbers (pairs of integers), as well as amplitudes (scalar) and phase shifts (angle) used in [Figure 2](#).

Problem (11) has the following analytical solution:

$$u(x, t) = \left(\cos(\theta(x, t)), \sin(\theta(x, t)) \right) \quad (13)$$

where $x = (x_1, x_2)$ and θ is a solution of the *linear* wave equation

$$\theta_{tt} - \Delta\theta = 0.$$

Such solutions are superpositions of the functions

$$\theta_k(x, t) := a_k \cos(k_1 x_1 + k_2 x_2 - \|k\|t - \varphi_k), \quad (14)$$

where $k = (k_1, k_2) \in \mathbb{Z}^2$ is the wavenumber, $a_k \in \mathbb{R}$ is the amplitude, and $\varphi_k \in \mathbb{T}$ is an arbitrary phase shift.

In the following numerical experiments, we thus compute the exact solution of our wave map problem (11) using formulas (13) and (14) and choosing the values a_k , φ_k from [Table 1](#).

We now use our multi-symplectic numerical method (12). [Figure 2](#) shows a plot of the error, i.e., the norm of the difference between the computed solution and the exact solution. The norm used is that of the space $L^\infty(0, T; L^2(\mathbb{T}^2))$, where \mathbb{T}^2 is the spatial domain, the two-dimensional torus. The integer N denotes the number of points in space. The final time is $T = 1$. We choose a Courant ratio $\Delta t / \Delta x = 1/2$, i.e., there are twice as many time points than space points. The slope of the fitted grey line is 2.15 which indicates convergence of order two.

[Figure 3](#) displays the relative energy error between the energy E and the initial energy $E_0 = 66.3$, along the numerical solution given by the multi-symplectic scheme (12) on the time interval $[0, 11]$ with $N = 2^7$ points in space. We observe good approximate energy conservation.

4.2. Breather solutions

We now consider breather solutions of the wave map equation

$$\begin{aligned} u_{tt} - u_{xx} &= \lambda u \\ |u|^2 &= 1, \end{aligned}$$

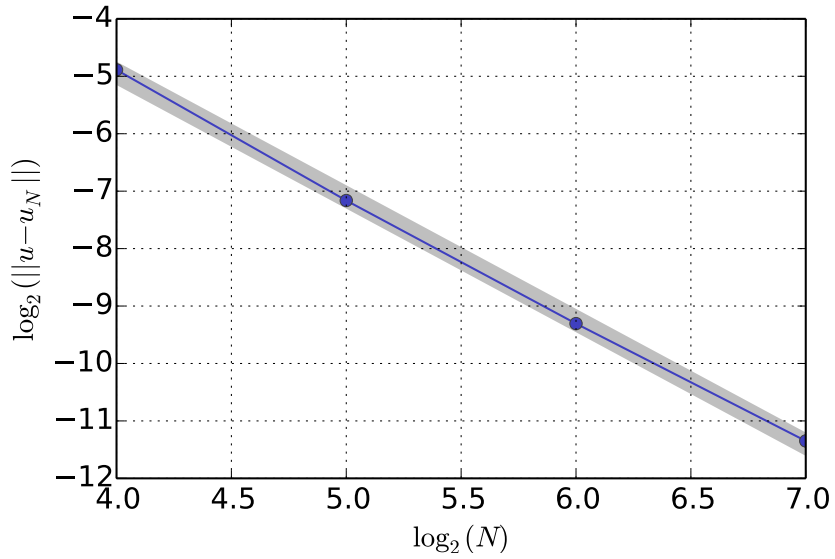


Figure 2: Wave map from the torus \mathbb{T}^2 to the circle: plot of the error of the computed solution with respect to the exact one. The integer N denotes the number of points in space. The slope of the fitted grey line is 2.15 which indicates convergence of order two.

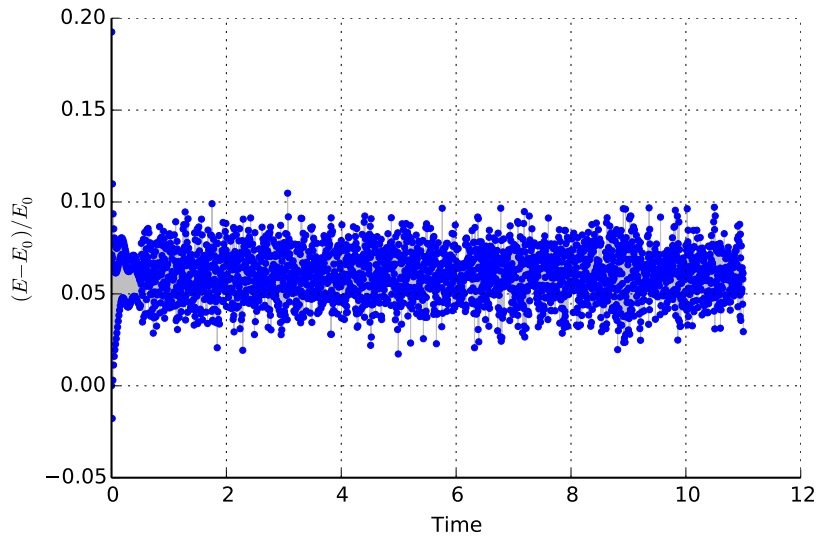


Figure 3: Wave map from the torus \mathbb{T}^2 to the circle: relative energy error $(E - E_0)/E_0$ along the numerical solution on the time interval $[0, 11]$. The initial energy is $E_0 = 66.3$.

where $u: \mathbb{R} \times \mathbb{T} \rightarrow \mathbb{R}^3$. We consider the following initial condition

$$u_0 = \begin{pmatrix} \cos(\ell x) \\ \sin(\ell x) \\ 0 \end{pmatrix} \quad (15a)$$

$$u_1 = u_0 + \begin{pmatrix} 0 \\ 0 \\ \varepsilon \sin(jx) \end{pmatrix}, \quad (15b)$$

where ℓ and j are integers such that $1 \leq j \leq \ell - 1$, and ε is an arbitrary small parameter. Observe that the period of the breather wave map tends to infinity when ε goes to zero.

Let us first show that this initial condition is a first order approximation of the breather wave map given by [27, Lemma 7.2]. Indeed, this breather wave map is given by

$$u_b(x, s) := \begin{pmatrix} \cos(\kappa) \cos(\ell x - \kappa) - \sin(\kappa) \cos(s/\sin(\kappa)) \sin(\ell x - \kappa) \\ \cos(\kappa) \sin(\ell x - \kappa) + \sin(\kappa) \cos(s/\sin(\kappa)) \cos(\ell x - \kappa) \\ \sin(\kappa) \sin(s/\sin(\kappa)) \end{pmatrix},$$

where

$$\tan(\kappa) = \frac{\ell}{j} \tan(jx) \quad \text{and} \quad s(x, t) := \int_{-\infty}^t \ell \sin(\alpha(\tau, x)/2) d\tau$$

and

$$\alpha = \alpha(x, t) = 4 \arctan\left(\frac{\sqrt{\ell^2 - j^2}}{j} \frac{\sin(jx)}{\cosh(\sqrt{\ell^2 - j^2}t)}\right)$$

is the classical breather solution of the generalised sine-Gordon equation $\alpha_{tt} - \alpha_{xx} - \ell^2 \sin(\alpha) = 0$.

In fact, the initial condition (15) is obtained using a first order approximation of $u_b(x, s)$ at $s = 0$. First, as noted in [27], using the identity for the sum of angles of trigonometric functions, the value of $u_b(x, 0)$ simply reduces to (15a).

Now, for $t \simeq -\infty$, we have $\cosh(\sqrt{\ell^2 - j^2}t) \simeq \infty$, so we approximate $\alpha(x, t)$ by

$$\alpha(x, t) \simeq 4 \frac{\sqrt{\ell^2 - j^2}}{j} \exp(\sqrt{\ell^2 - j^2}t) \sin(jx).$$

This gives in turn

$$s(x, t) \simeq \int_{-\infty}^t \frac{\ell}{2} \alpha(x, \tau) d\tau$$

so we obtain

$$s(x, t) \simeq 2 \frac{\ell}{j} \exp(\sqrt{\ell^2 - j^2}t) \sin(jx),$$

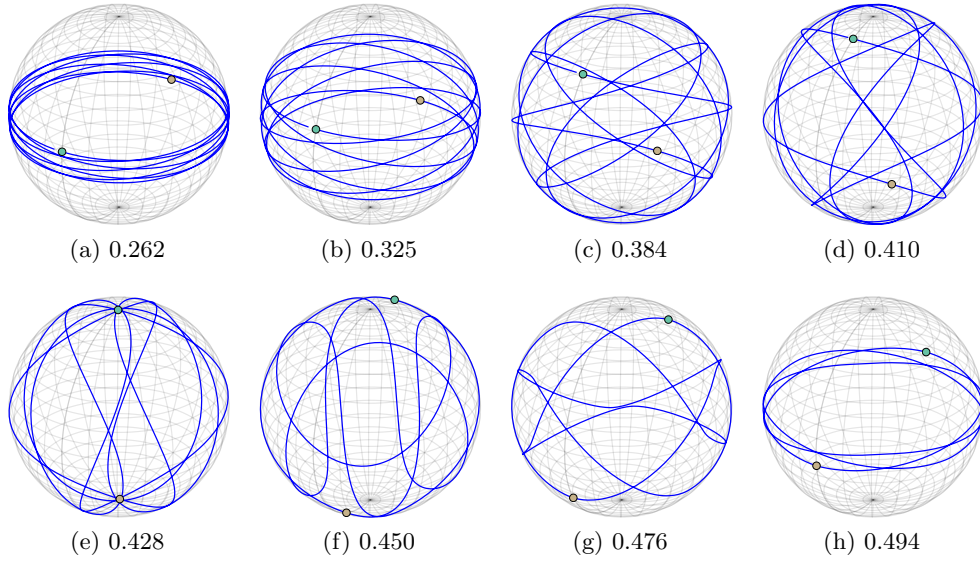


Figure 4: Wave map from the circle to the sphere: snapshots of the breather of winding number $\ell = 7$ and initial frequency $j = 5$. The caption below each snapshot indicates the time in period units. One can further see that each particle stays on a circle on the sphere, thus illustrating [27, Lemma 7.1].

and we choose

$$\varepsilon := 2 \frac{\ell}{j} \exp(\sqrt{\ell^2 - j^2} t),$$

which is infinitesimally small when $t \simeq -\infty$.

Finally, a first order development of u_b at $s = 0$ yields

$$u_b(x, s) \simeq u_b(x, 0) + \begin{pmatrix} 0 \\ 0 \\ s \end{pmatrix}$$

which justifies the choice (15b).

We now run our multi-symplectic scheme (9) on the example corresponding to the winding number $\ell = 7$ and the initial frequency $j = 5$. The value of ε in (15b) is set to 10^{-4} . Figure 4 presents snapshots of the numerical solutions computed with $N = 2^9$ points in space, and a Courant ratio $\Delta t / \Delta x = 1/2$. We observe a periodic motion, which leads us to define a *period* as the first time at which the numerical solution returns to its initial state.

Using the same data as in the previous numerical experiments, Figure 5 displays the relative energy error and amplitude in the z direction of the numerical solution over three periods. These plots, in period units, show, as expected, that the breathers are not stable. Note that it is a major merit of the proposed numerical method to be able to accurately compute the breather over a few periods.

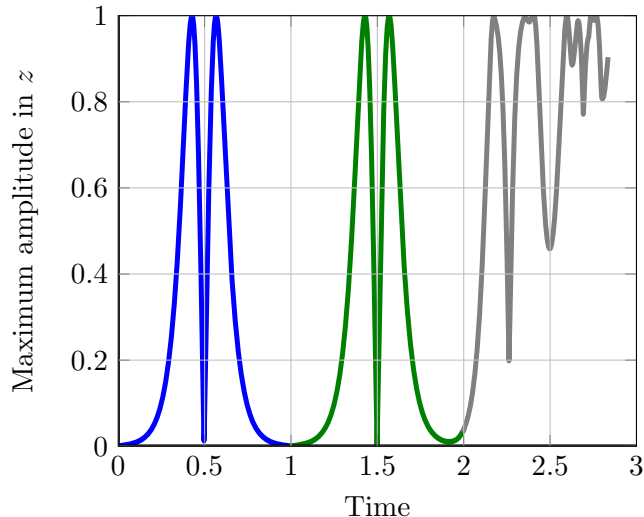


Figure 5: Wave map from the circle to the sphere: plot of the maximum amplitude in the z direction over three periods. Each period is plotted with a different colour. Observe how the proposed numerical method accurately computes the breathers over a few periods, despite the instability of the solutions.

Finally, Figure 6 shows the relative energy error of the above breather over thirty period units. We use the same colours as in Figure 5. The initial energy is still $E_0 = 967$, so we see that the energy oscillations are minimal, and that there is no energy drift.

4.3. Blow-up of smooth initial data

The purpose of this section is to show that our scheme obtains the same blow-up time as in the numerical experiments presented in [3, 15]. This is only a preliminary study and one should be aware that adaptive mesh refinement techniques, [9] for example, should be used in order to have a proper understanding of the behaviour of the solution close to blow-up times.

We consider the wave map equation

$$\begin{aligned} u_{tt} - \Delta u &= \lambda u \\ |u|^2 &= 1, \end{aligned}$$

where $u = u(x, t) \in \mathbb{R}^3$, $x = (x_1, x_2) \in [-1/2, 1/2]^2$. This problem is supplemented with homogeneous Neumann boundary conditions.

We consider the equivariant initial data [3, 15]

$$u_0(x_1, x_2) = \frac{1}{a(r)^2 + r^2} \left(2x_1 a(r), 2x_2 a(r), a(r)^2 - r^2 \right)$$

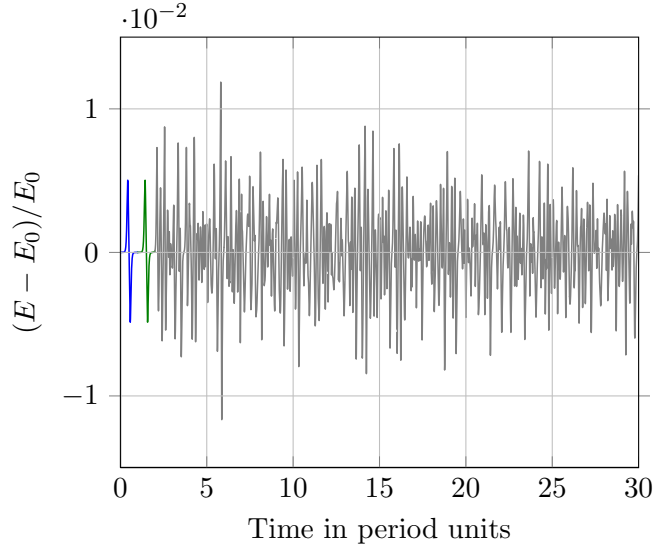


Figure 6: Wave map from the circle to the sphere: plot of the relative energy error $(E - E_0)/E_0$ of the breather of Figure 5 over thirty period units. We observe no energy drift.

with $r = \sqrt{x_1^2 + x_2^2}$ and

$$a(r) = \begin{cases} (1 - 2r)^4 & r \leq 1/2 \\ 0 & r \geq 1/2. \end{cases}$$

We use our multi-symplectic scheme with $N = 128$ points in each direction in space, with a Courant ratio $\Delta t/\Delta x = 1/2$. Our results are shown in Figure 7 and Figure 8. Looking at the two subplots of Figure 7, we can estimate the blow-up time at 0.28 by glancing at the maximum value of the computed energy. This corresponds to the time where the center particle brutally flips over to pointing to the opposite direction $z = -1$. Figure 8 offers a view of the z coordinate versus a radius. Once again we observe the blow-up time at 0.28 represented by a red horizontal line.

The blow-up time measured in Figure 7a at 0.28, as well as the flip observed in Figure 7b are identical to the ones observed in [3, 15].

4.4. Wave map equations with smooth potential

Finally, we consider the discretisation of a wave map equation with an additional smooth potential

$$V(u) = 400(u_1^2 + u_2^2).$$

The setting is otherwise the same as in §4.2. We plot some snapshots of the numerical solution given by our multi-symplectic integrator in Figure 9. The initial condition is a single winding around a great circle of the sphere, tilted from the equator plane at an angle of 45 degrees. It is thus a fixed point of the wave map without potential. That

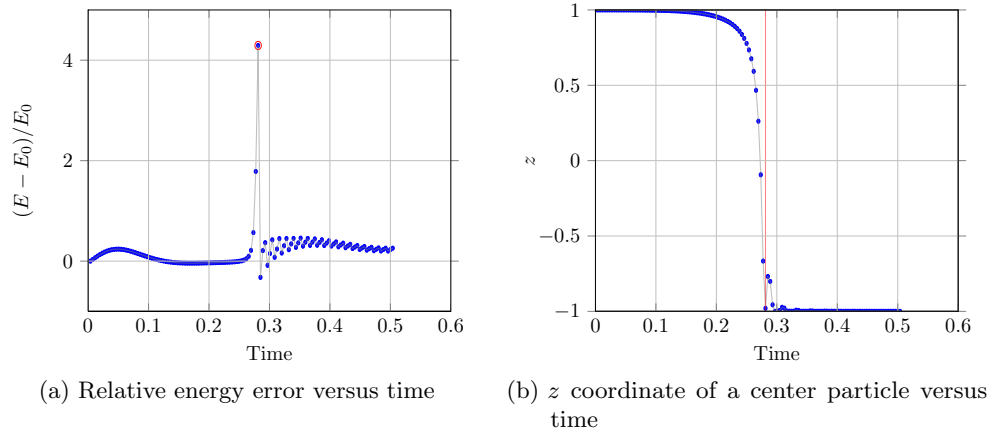


Figure 7: Blow-up of smooth initial data (4.3).

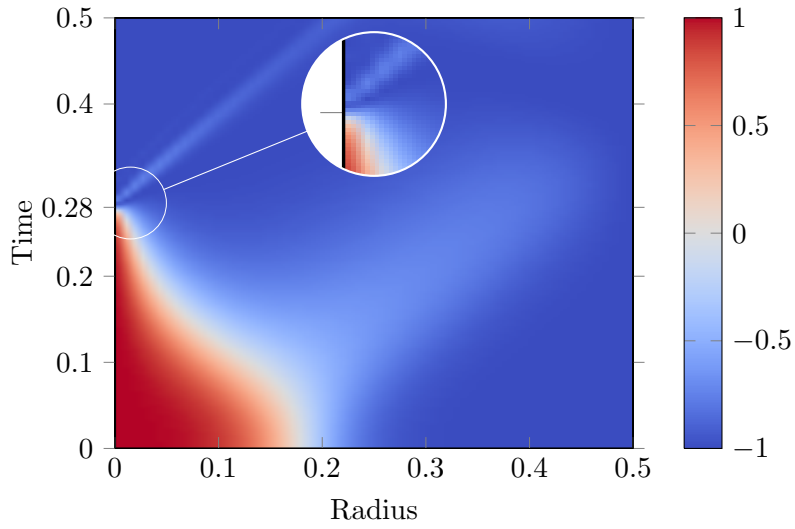


Figure 8: Blow-up: view of the z coordinate over time, versus a radius. The blow-up time, represented by the horizontal line, is 0.28, confirming the experimental measurements from the literature.

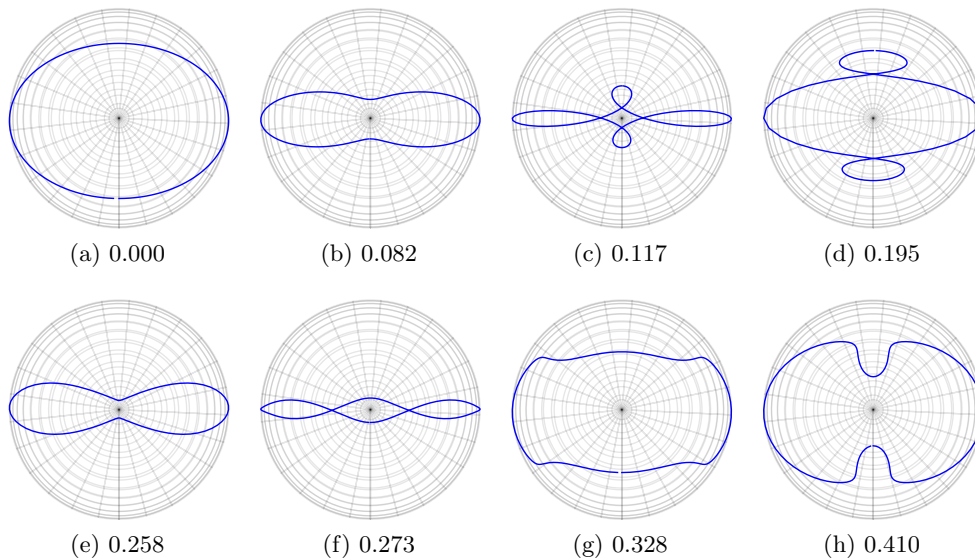


Figure 9: Wave map with potential: snapshots of the wave map equation with the potential (4.4). The caption below each snapshot is the time.

initial condition is not a fixed point of the wave map with potential, as is evidenced by the snapshots in Figure 9.

4.5. Wave map equations on a hyperbolic space

We use the hyperboloid model of the two-dimensional hyperbolic space. The ambient space is \mathbb{R}^3 with the bilinear form of signature $(-, -, +)$, i.e.,

$$\|(x, y, z)\| := -x^2 - y^2 + z^2.$$

We represent the solutions of the wave map with the *Poincaré disk* as a target. Recall that the Poincaré disk is a stereographic projection of the hyperboloid on a disk of radius one. A point of coordinates (x, y, z) is projected to the point $(x/(1+z), y/(1+z))$.

Our method works exactly in the same way, and the equation $\|u\|$ now represents the “sphere” associated with that bilinear product, that is a two-sheet hyperboloid. We always stay on the hyperboloid sheet with positive z -coordinate.

In Figure 10, we show the evolution of a wave map on the Poincaré disk, with initial condition, on the Poincaré disk identified as a subset of \mathbb{C} , given by

$$z_0(\theta) = e^{i\theta} + 0.3e^{i8\theta} + 0.2e^{i4\theta} \quad \theta \in [0, 2\pi].$$

Note that the simulation does not take place directly on the Poincaré disk, but on the upper hyperbolic sheet, as it is a Riemannian submanifold of \mathbb{R}^3 . We also show an energy plot on Figure 11 which confirms that there is no energy drift along the numerical solution.

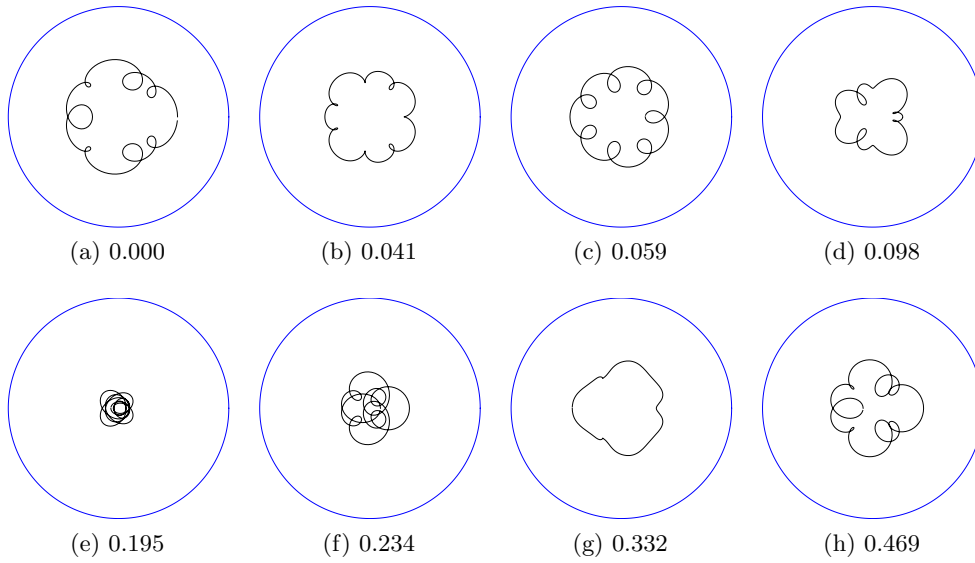


Figure 10: Wave map on a Poincaré disk. The caption below each snapshot is the time. In particular, the first plot represents the initial condition. There are $N = 2^8$ points, so the space step is $\Delta x = 1/N$, and we choose the time step $\Delta t = 0.5\Delta x$. Note that the numerical solution is surprisingly stable, developing no chaotic behaviour. As this seems independent of the chosen initial condition, this could indicate some general integrability property of the wave map with a hyperbolic plane target.

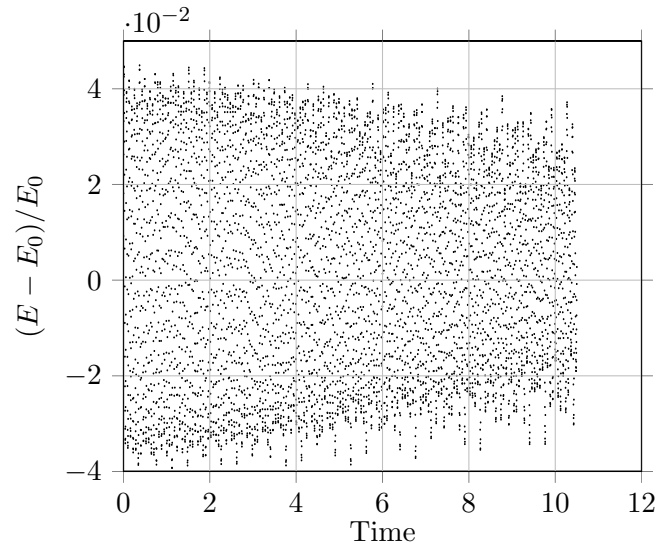


Figure 11: Relative energy plot of the simulation of Figure 10. The initial energy is $E_0 = -123$.

5. Conclusion and open problems

In this paper, we have proposed and studied a new multi-symplectic numerical integrators for wave map equations on the sphere. This numerical scheme is explicit, conserves the constraint, has good conservation properties and can be seen as a generalisation of the SHAKE algorithm for constrained mechanical systems. Furthermore, we observe convergence of order 2 for smooth solutions.

Our method allows to treat wave map equations with other target manifolds which are submanifolds of \mathbb{R}^n , see also [Appendix A](#). Such examples could include classical Lie groups and symmetric spaces, see for instance [36]. But these are nontrivial extensions that may be the subject of future investigations. Furthermore, it would also be interesting to understand whether different splitting of the multi-symplectic matrices could have some effect on the numerical discretisation. In addition, it remains to develop, to try out and further analyse other classical multi-symplectic schemes such as the Preissman box scheme or some multi-symplectic Runge–Kutta collocation methods. Such generalisations for constrained Hamiltonian PDEs seem far from straightforward.

For all these reasons, it seems to us that it would be of interest to get more insight into the behaviour of multi-symplectic schemes for Hamiltonian PDEs with constraints as derived in this publication.

A. Simulations on a complex projective space

We explain how to use our method to simulate wave maps with target given by the complex projective space. One possible application is to simulate the breathers described in [36, Example 8.2].

Our method needs the target manifold to be embedded as a submanifold of a Euclidean or Minkowski space. In this case, we use the embedding of $\mathbb{C}P^n$ in $S(n+1)$, the space of complex-symmetric (Hermitian) square matrices of size $n+1$. That space is equipped with the Frobenius scalar product $(\rho_1, \rho_2) := \text{Tr}(\rho_1 \rho_2)$.

The complex projective space is defined as the submanifold

$$\mathbb{C}P^n := \{ \rho \in S(n+1) \mid \rho^2 = \rho \quad \text{Tr}(\rho) = 1 \}. \quad (16)$$

The standard definition of $\mathbb{C}P^n$ is by quotienting a vector $\Psi \in \mathbb{C}^{n+1}$ by the equivalence relation $\Psi_1 \simeq \Psi_2 := [\exists \lambda \in \mathbb{C} \quad \Psi_2 = \lambda \Psi_1]$. The map sending the standard representation of $\mathbb{C}P^n$ to the one described above in (16) is simply $\Psi \rightarrow \Psi \Psi^*$, where we identify Ψ with a $(n+1) \times 1$ complex matrix (“column vector”), and where Ψ^* denotes the conjugate transpose of the matrix Ψ .

The only issue is that of the projection on $\mathbb{C}P^n$. Note that it is only a practical issue, as this setting already fits our framework exactly.

The constraint function is now defined on $S(n+1)$, is given by

$$g(\rho) = (\rho^2 - \rho, \text{Tr}(\rho) - 1),$$

and takes values in $S(n+1) \times \mathbb{C}$.

We observe that the second constraint is linear, so it will be automatically fulfilled by our method. In practice, it can be ignored entirely.

At the projection step, we want to project an element $\tilde{\rho} \in S(n+1)$ onto $\mathbb{C}P^n$ along the direction $\nabla g(\rho_0)$, and we may assume that $\text{Tr}(\tilde{\rho}) = 1$, i.e., the second constraint is already fulfilled. The result of the projection is $\rho \in \mathbb{C}P^n$. By differentiating g , the relation between ρ , $\tilde{\rho}$ and ρ_0 is thus

$$\rho = \tilde{\rho} + \rho_0 \Lambda + \Lambda \rho_0, \quad (17)$$

where $\Lambda \in S(n+1)$ is an unknown matrix. We thus see that we will have $(n+1)^2/2$ real unknowns.

We now impose the constraint, and this gives the quadratic equation in the matrix Λ :

$$\tilde{\rho}^2 - \tilde{\rho} + \tilde{\rho} \Lambda + \Lambda \tilde{\rho} + \Lambda^2 - \Lambda = 0. \quad (18)$$

Solving Λ in (18), and using it in (17) now gives the projected value $\rho \in \mathbb{C}P^n$.

Acknowledgements

DC acknowledges support from UMIT Research Lab at Umeå University. OV acknowledges support from the J.C. Kempe memorial fund (grant no. SMK-1238).

References

- [1] L. Bañas, A. Prohl, and R. Schätzle. Finite element approximations of harmonic map heat flows and wave maps into spheres of nonconstant radii. *Numer. Math.*, 115(3):395–432, 2010.
- [2] S. Bartels. Semi-implicit approximation of wave maps into smooth or convex surfaces. *SIAM J. Numer. Anal.*, 47(5):3486–3506, 2009.
- [3] S. Bartels, X. Feng, and A. Prohl. Finite element approximations of wave maps into spheres. *SIAM J. Numer. Anal.*, 46(1):61–87, 2007/08.
- [4] S. Bartels, Ch. Lubich, and A. Prohl. Convergent discretization of heat and wave map flows to spheres using approximate discrete Lagrange multipliers. *Math. Comp.*, 78(267):1269–1292, 2009.
- [5] B. K. Berger, P. T. Chruściel, and V. Moncrief. On “asymptotically flat” space-times with G_2 -invariant Cauchy surfaces. *Ann. Physics*, 237(2):322–354, 1995.
- [6] P. Bizoń, T. Chmaj, and Z. Tabor. Formation of singularities for equivariant $(2+1)$ -dimensional wave maps into the 2-sphere. *Nonlinearity*, 14(5):1041–1053, 2001.
- [7] J. Bridges, T. Multi-symplectic structures and wave propagation. *Math. Proc. Cambridge Philos. Soc.*, 121(1):147–190, 1997.

- [8] T. J. Bridges and S. Reich. Multi-symplectic integrators: numerical schemes for Hamiltonian PDEs that conserve symplecticity. *Phys. Lett. A*, 284(4-5):184–193, 2001.
- [9] C. J. Budd, W. Huang, and R. D. Russell. Moving mesh methods for problems with blow-up. *SIAM J. Sci. Comput.*, 17(2):305–327, 1996.
- [10] J. Frauendiener and R. Peter. Blow-up of the nonequivariant $(2 + 1)$ -dimensional wave map. *ANZIAM J.*, 55(2):151–161, 2013.
- [11] V. Georgiev and A. Ivanov. Concentration of local energy for two-dimensional wave maps. *Rend. Istit. Mat. Univ. Trieste*, 35(1-2):195–235 (2004), 2003.
- [12] M. J. Gotay. A multisymplectic framework for classical field theory and the calculus of variations. I. Covariant Hamiltonian formalism. In *Mechanics, analysis and geometry: 200 years after Lagrange*, North-Holland Delta Ser., pages 203–235. North-Holland, Amsterdam, 1991.
- [13] E. Hairer, C. Lubich, and G. Wanner. *Geometric Numerical Integration*, volume 31. Springer-Verlag, second edition, 2006. Structure-preserving algorithms for ordinary differential equations.
- [14] J. Isenberg and S. L. Liebling. Singularity formation in $2 + 1$ wave maps. *J. Math. Phys.*, 43(1):678–683, 2002.
- [15] T. K. Karper and F. Weber. A new angular momentum method for computing wave maps into spheres. *SIAM J. Numer. Anal.*, 52(4):2073–2091, 2014.
- [16] M. Keel and T. Tao. Local and global well-posedness of wave maps on \mathbf{R}^{1+1} for rough data. *Internat. Math. Res. Notices*, (21):1117–1156, 1998.
- [17] J. Krieger. Global regularity and singularity development for wave maps. In *Surveys in differential geometry. Vol. XII. Geometric flows*, volume 12 of *Surv. Differ. Geom.*, pages 167–201. Int. Press, Somerville, MA, 2008.
- [18] J. Krieger, W. Schlag, and D. Tataru. Renormalization and blow up for charge one equivariant critical wave maps. *Invent. Math.*, 171(3):543–615, 2008.
- [19] B. Leimkuhler and S. Reich. *Simulating Hamiltonian dynamics*, volume 14 of *Cambridge Monographs on Applied and Computational Mathematics*. Cambridge University Press, Cambridge, 2004.
- [20] J. E. Marsden, G. W. Patrick, and S. Shkoller. Multisymplectic geometry, variational integrators, and nonlinear PDEs. *Comm. Math. Phys.*, 199(2):351–395, 1998.
- [21] R. I. McLachlan, K. Modin, O. Verdier, and M. Wilkins. Geometric Generalisations of Shake and Rattle. *Found. Comput. Math.*, 14(2):339–370, 2014.

- [22] B. Moore and S. Reich. Backward error analysis for multi-symplectic integration methods. *Numer. Math.*, 95(4):625–652, 2003.
- [23] R. Peter and J. Frauendiener. Free versus constrained evolution of the $2 + 1$ equivariant wave map. *J. Phys. A*, 45(5):055201, 19, 2012.
- [24] K. Pohlmeyer. Integrable Hamiltonian systems and interactions through quadratic constraints. *Comm. Math. Phys.*, 46(3):207–221, 1976.
- [25] H. Ringström. On a wave map equation arising in general relativity. *Comm. Pure Appl. Math.*, 57(5):657–703, 2004.
- [26] W. Seiler. *Involution. The formal theory of differential equations and its applications in computer algebra*. Springer, 2010.
- [27] J. Shatah and W. Strauss. Breathers as homoclinic geometric wave maps. *Phys. D*, 99(2-3):113–133, 1996.
- [28] J. Shatah and M. Struwe. *Geometric wave equations*, volume 2 of *Courant Lecture Notes in Mathematics*. New York University, Courant Institute of Mathematical Sciences, New York; American Mathematical Society, Providence, RI, 1998.
- [29] J. Shatah and M. Struwe. The Cauchy problem for wave maps. *Int. Math. Res. Not.*, (11):555–571, 2002.
- [30] J. Shatah and C. Zeng. Constrained wave equations and wave maps. *Comm. Math. Phys.*, 239(3):383–404, 2003.
- [31] M. Struwe. Wave maps. In *Nonlinear partial differential equations in geometry and physics (Knoxville, TN, 1995)*, volume 29, pages 113–153. Birkhäuser, Basel, 1997.
- [32] T. Tao. Ill-posedness for one-dimensional wave maps at the critical regularity. *Amer. J. Math.*, 122(3):451–463, 2000.
- [33] T. Tao. Global regularity of wave maps. ii. small energy in two dimensions. *Comm. Math. Phys.*, 224(2):443–544, 2001.
- [34] D. Tataru. The wave maps equation. *Bull. Amer. Math. Soc. (N.S.)*, 41(2):185–204 (electronic), 2004.
- [35] D. Tataru. Rough solutions for the wave maps equation. *Amer. J. Math.*, 127(2):293–377, 2005.
- [36] C.-L. Terng and K. Uhlenbeck. $1 + 1$ wave maps into symmetric spaces. *Comm. Anal. Geom.*, 12(1-2):345–388, 2004.
- [37] O. Verdier. Reductions of Operator Pencils. *Math. Comp.*, 83:189–214, 2014.
- [38] J. Zhai, J. Fang, and L. Li. Wave map with potential and hypersurface flow. *Discrete Contin. Dyn. Syst.*, (suppl.):940–946, 2005.